Journal of Machine Engineering, 2026, Vol. 26
ISSN 1895-7595 (Print) ISSN 2391-8071 (Online)

Received*: 16 June 2026* / Accepted: *21 October 2026* / Published online: *27 November 2026*

CAM,
robotics,
quality inspection,
forging

Christian NAUMANN[1,2*], Martin NAUMANN[1],
Klara SCHUBERT[1], Leutrim GJAKOVA[1],
Philipp KLIMANT[1], Martin DIX[3,4]

AUTOMATED QUALITY MONITORING OF HOT FORGINGS BY ROBOT-HELD LASER SCANNER MEASUREMENT

Forging is still one of the main production processes in automotive, railway and airplane manufacturing. Forging produces very little waste and improves the material durability during the forming process. The downside is the low accuracy and the need for subsequent cutting processes to create the more precise geometric features of the workpiece. Due to the low accuracy, there is always a compromise between how much material to add to ensure that the final dimensions can still be met and the need to remove that additional material in the subsequent cutting operations. A large problem for die forging, particularly for small and medium batch sizes is that it takes a long time for the workpiece to cool down enough that the resulting geometry can be measured against the desired CAD dimensions. During this time, much scrap may be produced. This paper demonstrates a method for measuring hot workpieces immediately after forging using a robot-held laser scanner. The method is demonstrated on forged pieces to assess its feasibility, duration and precision.

1. INTRODUCTION AND STATE OF THE ART

FORGING is still one of the main production processes in automotive, railway and airplane manufacturing. Forging produces very little waste and improves the material durability during the forming process. The downside is the low accuracy and the need for subsequent cutting processes to create the more precise geometric features of the workpiece. The most common types of defects in die forging are [1, 2]:

- Unfilled sections: the part does not completely fill the die. This can happen, e.g., when there is not enough raw material, when there are too few hammers strikes or when the material is too cold to begin with.
- Cold shut: small crack or seam often near corners or sharp surface curvatures. This can happen due to the die geometry or because of suboptimal cooling.

[1] Automation and Monitoring, Fraunhofer IWU Chemnitz, Germany
[2] Virtual Technologies, Hochschule Mittweida University of Applied Sciences, Germany
[3] Production Systems and Processes, Chemnitz University of Technology, Germany
[4] Process Technology, Fraunhofer IWU Chemnitz, Germany
[*] E-mail: christian.naumann@iwu.fraunhofer.de
https://doi.org/10.36897/jme/241994

- Scale pits: surface defects due to left-over scale in the die, which is hammered into the following workpiece. This can usually be avoided by cleaning the die after forging.
- Die shift: a mismatch between upper and lower die.
- Flakes: oxide scales forming on the surface of the workpiece. This always happens to a certain degree but also depends on the cooling rate.
- Surface cracking: cracks on the surface of the workpiece. This is usually a result of a too low forging temperature.

Which specific defects and threshold are used to determine whether a part passes or fails, depends on the specific requirements of the workpiece and its final application. Some defects can easily be identified by manual visual inspection, while others are more subtle or depend on specific numeric thresholds. One of these quality indicators is the geometric precision. This is important in sections where the workpiece is subsequently milled to produce smooth functional surfaces, or sections where the durability of the material needs to meet specific requirements. If these sections have less material than they should, then the part cannot be salvaged and becomes scrap.

A large problem for die forging, particularly for small and medium batch sizes is that it takes a long time for the workpiece to cool down enough that the resulting geometry can be measured against the desired CAD dimensions. During this time, much scrap may be produced. Obviously, waiting on the production of the second workpiece, while the first one cools down enough to be measured properly, is not a viable option. Also, even if this was done and part one passed inspection, there is still no guarantee that subsequent parts will also pass. Even in very well designed and executed forging processes, effects such as small fluctuations in material or process parameters and especially die degradation can lead to defects during series production [3]. Therefore, measuring the workpiece while it is still hot, would be the best option to significantly reduce scrap and thereby save on energy and CO_2 emissions. Ideally, this measurement should be automated and fast enough to check every or at least every second or third workpiece to ensure consistent quality. Naturally, hardware costs and safety considerations are also important.

Quality inspection for forged workpieces can generally be done with a number of different sensors and methods. A very basic method, which is often used in the field, is the use of a simple mechanical gauge shaped like a two-pronged fork. This gauge can be used directly on the hot workpiece to check the thickness of a certain section or a cylindrical diameter. Thus, this method provides very little information on the overall geometry of the workpiece.

Another option often used for high-precision workpiece inspection is via touch probes. Usually, a spherical probe is brought into contact with the workpiece surface, and the probe position is recorded. There are different realizations of this measurement principle such as coordinate measurement machines, hand-held probes which are optically tracked (e.g. GOM touch probes), hand-held robotic arms (e.g. FARO arm) and laser trackers, which use independent spherical reflectors. However, their use for measuring free-form objects is somewhat limited, because they only record the position of the probe center and then try to compensate for the radius in a specified direction. Contacting probes also typically do not work for hot workpieces.

Therefore, optical measurements, with the sensor at a larger distance from the workpiece offer the best option. Here too, there are several different measuring strategies, such as laser scanners, structured light scanners and industrial CT scanners. One example for this is stereo-imaging using the ExaScanner from Creaform3D, which is used by Reicher for 3D free-form scanning as a precursor step to robot-based workpiece inspection. The scanner determines the geometry, which is then used to calculate a scanning path for the robot [4]. Thereby, subsequent similar workpieces can be scanned automatically using a robot-held camera.

Another option is laser triangulation, where a workpiece is scanned via individual scan lines. For each point within the line, the x- and z- coordinates of the geometry are measured. Then, the line is moved incrementally in the y-direction across the workpiece. By recording the corresponding y-position of the scan line for each scanned line, a 3D map of the entire workpiece can be created. Therefore, the exact location of the scanner needs to be known at all times. Here, the scanner is attached to the robot's manipulator so that the robot control, with some constant offset, provides the scanner position. An interesting alternative is presented by Brosed et al., who use the robot to position the workpiece in discrete locations and move the laser scanner on a highly precise linear axis [5]. The discrete robot locations are measured precisely using a calibration routine, where the robot holds a calibration board containing known calibration points and planes.

Mejia-Parra et al. present an in-line optical inspection system for hot forged workpieces using two cameras with laser line projectors and a pyrometer to measure the workpiece temperature, which is typically around 600°C [6]. The system is capable of automatically measuring the circular runout of warm revolution workpieces in less than a minute and thereby reduces the number of defective workpieces by 95% via early process adjustments.

Lazarevic et al. compare different measurement systems for the optical inspection of cutting parts [7]. They use a coordinate measurement machine (CMM) as a reference and compare that to three different GOM ATOS structured light scanners. Their results show varying differences both between the scanners and compared to the CMM. However, the deviations mostly remained between 0.01 and 0.1mm for the measured cube-shaped parts.

Hawryluk and Ziemba provide a detailed overview of modern measurement techniques in hot die forging processes. Their review analyzes both thermal and geometric measurement equipment and challenges with a focus on die geometry and wear detection and process control [8].

Da Silva Santos et al. used a robot-held 2D laser line scanner to capture the geometry of small industrial sealed parts. They achieved an overall dimensional identification error of 0.34mm and with it, were able to reject non-compliant parts with a reliability of 96.6% [9].

Han et al. used marker-based stereo-localization to detect the workpiece location with an uncertainty of about 20µm [10]. In their experiments, a robot-held stereo-camera reliably detected the location of a workpiece fitted with specially designed markers in less than 7s.

Li et al. use enhanced phase measuring profilometry to measure the 3D surface topography during powder bed fusion additive manufacturing [11]. This method allowed them to monitor the printing process in real-time and detect various shape and surface defects. Their demonstrator used a fixed setup to monitor the entire printing workspace at once. Tian et. al. used a pulsed time-of-flight laser radar (Lidar) sensor system with two motors to measure the dimensions of large cylindrical hot forgings [12].

The motors are used to rotate the Lidar sensor to capture the workpiece geometry in 3D. This is done by measuring one point at a time, which requires a compromise between point density and measuring time. The sensor measures at large distances of over 15m, making the heat radiated by the forging less problematic for the sensor.

A similar approach is used by Bokhabrine et al., who measure very large hot metallic shells using two Leica ScanStation2 laser scanners at distances of about 15m [13]. The scanners produce large point clouds, from which background data needs to be removed, followed by a registration to match the data from both scanners. The resulting 3D geometry is accurate to about 8mm for workpieces of a diameter of over 5m, which is faster and more accurate than the previously used rulers with 25mm uncertainty.

Du and Du use a 2D laser range sensor (TLRS) to measure 3D geometries more efficiently [14]. The TLRS is attached to a servo motor to angle the scanning plane. The sensor produces a triangulated irregular network, which is optimized locally to simplify the computational complexity. Since both workpiece and sensor are stationary, the sensor only captures the visible part of the geometry and not a fully 3D model.

Liu et al. used a blue structured laser light projector and two cameras with band-pass filters to measure the diameter of large hot forgings. Some of their main challenges were resolving the light stripes using a modified Gaussian model and dealing with the perspective distortions of the laser lines on cylindrical workpieces. They achieved an accuracy of 0.8% relative diameter error [15] and 0.7% [16]. In a later investigation, their system reduced the absolute error to 0.32mm (0.27%) in their experiments [17]. Zhang et al. used a green line laser projector driven by a stepper motor on a linear axis together with a CCD camera to capture 3D geometrical data of large hot forgings [18]. Similar to Brosed et al., they use calibration artifacts to obtain the transformations from 2D image coordinates to 3D global coordinates. Particle swarm optimization is used to reduce the optical distortions. In their experiments, they achieve an accuracy of less than 1mm for section diameter measurements. A later work by Zhang et al. expanded the method to less regular shapes and achieved an accuracy of less than 4mm for a special shell cover of ca. 800mm diameter [19].

Zhao et al. use phase measurement profilometry with blue sinusoidal structured light to measure 3D free-form surfaces of hot objects [20]. A digital light processing projector is used together with a 3-CCD camera for separate filtered red, green and blue image data. A low pass filter applied to the blue color components is used to determine the order of the phase-shifting fringe pattern, which can be used to compute the unwrapped 3D geometry from multiple wrapped 2D maps. In their experiments, they measured a small hot glowing forging of size 63x114mm at a distance of 1.5m with a maximum error of 1.5mm.

Han et al. present a robot-driven 3D shape measurement system for the automatic quality inspection of hot forged parts in a production line [21]. They use a combination of a blue light filter and an infrared cut-off filter to block the radiation from the glowing workpiece and significantly reduce its impact on the 3D sensor. Additionally, they use a liquid cooling system to protect the inspection system from the heat and keep its temperature between 30 and 34°C during the inspection of 900°C warm parts. The distance between scanner and part is somewhere between 80 and 100cm, as shown in the corresponding YouTube video. In order to speed up the scanning process, which is limited by the data transmission rate, a time division multiplexing trigger is used.

Table 1. Overview on state of the art

Research Team / Year	Workpieces	Method / Technology	Precision	Speed	Remark / Limitations
Reicher 2011	small, irregular, cold	Robot-held 2D camera, 3D scanner	unknown	< 1min	Proof of concept
Brosed et al. 2011	small, irregular, cold	Laser scanner on linear axis with robot-held workpiece	< 0.1mm	25s	High precision, problematic for large, hot workpieces
Mejia-Parra et al. 2019	hot, revolution parts	Laser line projectors with two cameras	≤ 0.1mm	< 1min	Requires revolution geometries and clamping system, no full 3D scan
Lazarevic et al. 2019	cold parts with flat surfaces	Structured light scanners	≤ 0.1mm	presumably < 1min	Manual scans
Da Silva Santos et al. 2023	small, irregular, cold	Robot-held 2D laser line scanner	< 0.4mm	presumably < 1min	Not tested for full 3D geometry scanning
Li et al. 2018	Small, warm powder-bed fusion parts	Phase measuring profilometry	presumably < 0.1mm	real-time	Unclear precision, best for small, stationary, flat objects
Tian et al. 2009	Large, hot, cylindrical	Pulse time-of-flight Lidar	Ø < 2mm L < 7mm	< 1min	Suitable for large, cylindrical workpieces with large tolerances
Bokhabrine et al. 2012	Large, hot, cylindrical	Two laser scanners at large distance	< 8mm	faster than ruler-based	Suitable for large, cylindrical workpieces with large tolerances
Du and Du 2012	Medium to large, irregular, hot	2D laser range sensor on a servo motor	< 3mm	presumably < 1min	Only scans the visible face of a workpiece for a single location
Liu et al. 2016	hot, cylindrical	Structured light projector with two cameras	< 0.4mm	presumably fast	Unclear time requirement, suitable for cylindrical workpieces
Zhang et al. 2014	Large, hot, irregular	Line laser projector drive by stepper motor, CCD camera	< 4mm	faster than ruler-based	Relatively low point density good for rough dimensional inspections
Zhao et al. 2015	Small, hot, irregular	Digital light processing projector with 3-CCD camera	< 1.5mm	few seconds	Robust and relatively precise for small hot parts
Han et al. 2018	Hot, irregular parts	Robot-held 3D structured light scanner	unknown	< 1 min	Unknown precision but flexible and fast with good repeat accuracy

Since the scan data contained large amounts of noise, data registration was optimized using an adaptive distance threshold-based ICP algorithm with KD-tree to calculate point pair matches. The system scanned the parts in 10 discrete locations using a blue structure light scanner. The parts are scanned in a special holder, which places it in a similar position and orientation allowing for in-line inspection in less than 30 seconds plus another 13 seconds for data evaluation, which satisfies the 45s cycle time of the transfer line. The paper suggests a repeat accuracy of 0.1mm for cold parts, but it says little on the overall geometric accuracy of the system.

Table 1 summarizes the state of the art relevant to the quality inspection of hot parts. The listed precision may vary depending on the geometries scanned and may not apply to hot parts. It is also determined from very few sample measurements and only an indication. The inspection time depends on the size and shape of the workpiece and may not include times for part handling, measurement setup or data processing and evaluation. While the table indicates both a large interest in the subject and a multitude of existing solutions for part quality inspection, most systems still have significant limitations with some lacking in measurement precision.

The inspection system from Brosed et al. is suitable for workpieces, which are light and easy to grip, but excludes many others unless a very large robot is used. The workpieces considered here can be over 100kg, which is difficult to lift for most conventional robots.

The solution from Mejia-Parra, while impressive in terms of speed and accuracy, requires a fixed setup and substantial preparation for each type of workpiece measured and currently only supports a small set of revolution workpieces.

Similarly, most of the other presented solutions for 3D measurement lack either the required flexibility for handling a large variety of different workpieces or are too complicated or imprecise for the forged workpieces with higher quality requirements frequently used in the automotive, railway, aerospace or defence industry.

Another aspect, which most authors have ignored so far, is that the required dimensions are typically formulated for the cold workpiece, while the measurement should be performed on the hot workpiece, so that the thermal shrinkage needs to be considered.

This paper will present a new and more flexible approach to 3D scanning of hot forgings using a robot-held laser line scanner. Chapter 2 will present the initial requirements of the solution along with the design of the industrial demonstrator used to develop and test the inspection system. Chapter 3 describes the software and interfaces necessary for the automation of the scanning process. Chapter 4 presents the results of several measurements performed to determine the accuracy of the robot and of the scanned models. A summary and outlook conclude the paper.

2. QUALITY INSPECTION SYSTEM FOR HOT FORGED PARTS

RELIABLE QUALITY INSPECTION of hot forged parts depends on the expected workpiece geometries (form, size and weight), the local conditions in the production hall (space, temperature, vibration, logistics) and the specific requirements (cycle time, precision, temperature, degree of automation, price, etc.). For the current application, the following requirements were specified:

- Parts of varying shapes up to a size of 0.8m x 0.8m x 0.3m,
- Small to medium batch sizes, typically around 100 parts,
- Cycle time including logistics < 5min, ideally < 3min,
- Initial part temperature variable, up to 1000°C,
- Vibration-resistant measurements (other forges may be active at all times),
- Measurement room available near the forge with roughly 8m x 4m dimensions,
- Hardware cost < €100,000,
- Automated as much as possible, but manual intervention is acceptable so long as no great training is required and safety is guaranteed,
- Measurement uncertainty < 1mm, ideally < 0.5mm,
- Little or no effort for the setup of a new workpiece type.

These requirements present three main challenges: the practically unlimited workpiece spectrum, the high temperature and the short cycle time. Low costs and robust equipment are also very important to ensure the possibility of a broad industrial application of the solution in a branch of the industry, which is currently strained by tariffs, high energy cost and a struggling automobile industry. Since the work is publicly funded, research and development costs for the measurement system, the custom CAM software and the intensive commissioning and testing effort shall be ignored here.

In order to ensure high-precision surface detection of hot glowing parts, a blue (405nm) laser scanner of type MicroEpsilon LLT3000-100/BL was chosen. The sensor has a Z-axis linearity of 9µm and a maximum resolution of 2048 points per profile with a measuring frequency of up to 10 kHz. This makes LLT3000 generally suitable for the application, but the sensor is only one part of the system. Since the scanner has a z-range of 140-340mm and can operate only up to 40°C, a special cooling housing for the sensor was also used and connected to a small industrial water cooling unit. The cooling housing comes with safety glass to protect the scanner. Experiments with short scanning distances and high workpiece temperatures have led to the breaking of this glass due to the extremely high heat transfer from radiation. Therefore, the use of an infrared-filter as suggested by Han et al. will be employed in the next iteration [21].

For a maximum degree of automation, the sensor is attached to a robot arm, which can freely move the scanner around the workpiece. The industrial robot ABB IRB 2600 with a motion range of 1.65m and a carrying capacity of 20kg was chosen, together with an IRC5 robot controller and a Flexpendant user interface. The robot has a repeat accuracy of 0.04mm for positions and 0.13mm for paths. The maximum positioning uncertainty is rated at 0.65mm with an average of 0.25mm. To simplify the positioning of the workpiece with respect to the robot, a rotating table was also installed, on which the hot part is placed during the scanning operation. The table is not strictly necessary, but it improves the safety of the system and provides additional flexibility to the scanning operation.

One last component of the inspection system is a wall-mounted camera with bright LED lighting above the rotary table, which is used to determine the location and orientation of the workpiece on the table. In the future, an additional infrared camera or simply an RGB camera could be added to automatically estimate the workpiece temperature.

A protective fence and a light curtain are used to ensure that no personnel can reach the robot during the scanning operation. When the light fence is breached, such as during loading

and unloading operations, an emergency stop is triggered, which has to be manually revoked before any operations can resume.

The control cabinet and industrial PC for running the CAM software were placed in an enclosed side room to keep out flakes and particulates from the forging environment. The final setup of the entire measuring room can be seen in Fig. 1.

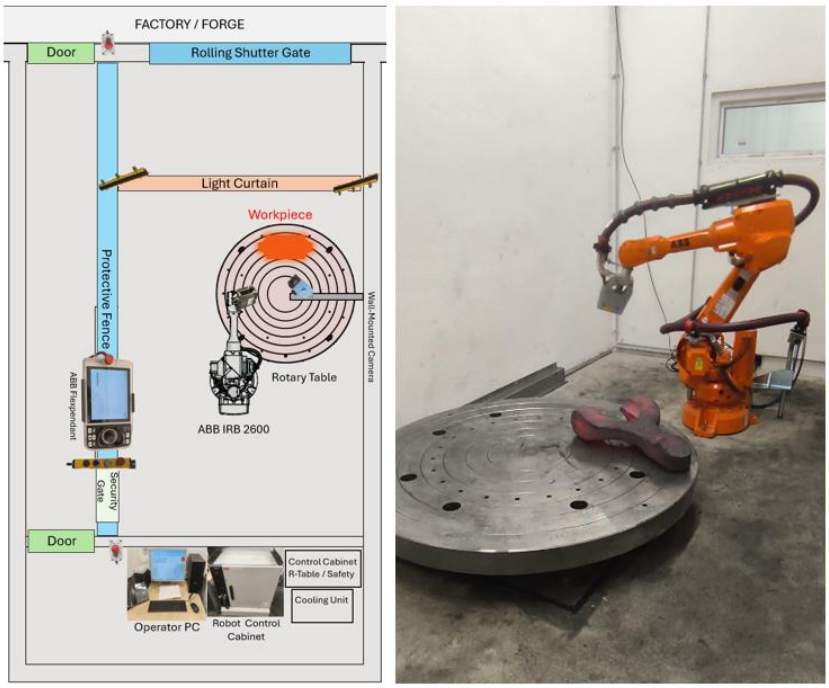


Fig. 1. Layout and picture of the measuring room adjacent to the factory floor

The scanning process is summarized in Fig. 2 and happens as follows:

1. Rolling shutter gate opens and a specialized forklift places the workpiece on the rotary table.
2. Forklift leaves the room, closes the gate, cancels the emergency stop and triggers the quality inspection via the operator PC.
3. The table is rotated by ca. 160° CCW for optimal reachability of the robot and scanner.
4. The camera takes a snapshot and determines the workpiece position and orientation.
5. The CAM software computes the scanning path comprised of a parallel grid pattern and uploads the created NC-file onto the robot control.
6. The robot performs the scan before returning to its home position.
7. The table rotates back to the loading position for unloading or overturning of the workpiece for 2-sided scanning.
8. The scanner and robot data are retrieved from the controllers.
9. Data synchronization, position transformation and correction, removal of background data and point cloud registration create a unified 3D point cloud of the workpiece.
10. Comparison to the desired 3D model of the workpiece via another registration yields the geometric deviation.
11. The next workpiece can be scanned or the production stopped in case of several consecutive failed parts.

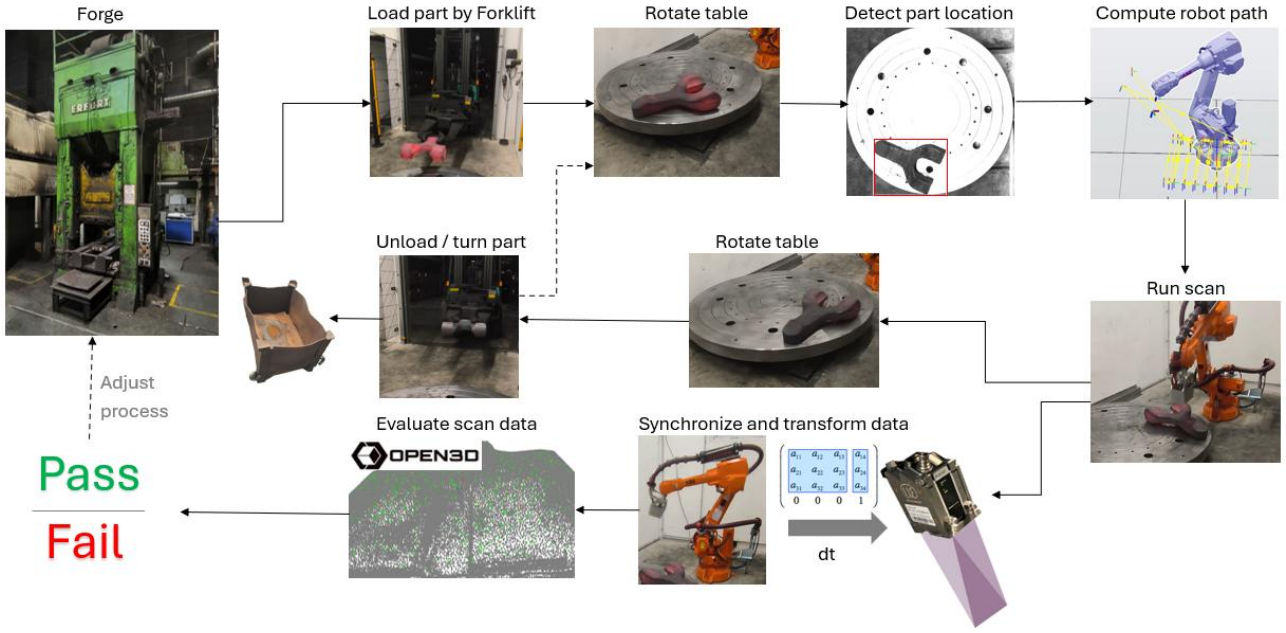


Fig. 2. Workflow of quality inspection via automated 3D scanning

At this point, the system has already revealed three weaknesses. The first is that the robot is barely large enough to scan large workpieces. A larger robot would have been better, though also more expensive. The robot is located 67cm from the edge of the table, which has a diameter of 1.6m. Thus, given that the robot needs to tilt the scanner around the workpiece, it can only scan roughly to the center of table. Placing the robot closer to the table would make it difficult to operate close to the table's edge on the side of the robot. This is, however, where the rotary table comes in handy, because parts of the workpiece which are difficult to scan can be avoided through rotations of the workpiece.

The second problem is that the ABB robot control makes it difficult to create tool paths through automated algorithms. Programming linear motions is possible but requires not only the knowledge of position and orientation (in quaternion notation), but also the axis quadrants for each robot pose. In practice, this requires an inverse transformation for all path points. Here, a proper NC controller would be ideal, though again more expensive.

The third problem is that the scanner and its supply cables and cooling tubes can cause collisions with the robot for certain combinations of the axes 4-6. This makes a completely automated workflow from position detection to path planning and execution risky, unless certain restrictions are posed or manual supervision is maintained.

3. QUALITY INSPECTION SOFTWARE AND ALGORITHMS

THE QUALITY INSPECTION SOFTWARE is the core of the inspection system, which performs all CAM operations, communication with the robot, scanner and camera, data processing and evaluation and which also contains the GUI for the operator to view and control all aspects of the inspection process.

The software contains four main tabs needed for the operation. The first one contains the settings, allowing the user to change the scan speed, the scanning grid pattern, data file naming conventions, number of evaluation points, point cloud registration thresholds and many more. The second tab is for workpiece management, where new workpieces can be added with details such as name, ID, dimensions, type, cold CAD model, warm CAD model, warm CAD model temperature, forging temperature and some others.

The third tab is for the system initialization, which contains all operations needed to start up the system. The tab contains buttons for scanning the network for the controllers, connecting to the controllers, initializing the controllers for scanning operations and table rotation commands. There is also a button for capturing the empty table surface.

The final tab is for the scanning process which contains buttons for rotating the table, detecting the workpiece location, computing the tool path, uploading the NC file to the robot control, starting the inspection, exporting the scan data, processing and finally evaluating the scan data. These buttons are arranged simply left to right so that an untrained operator only needs to go through all steps once per workpiece and then again for the next one. Theoretically, all steps could be linked automatically to run at the press of a single button, but the software is currently still in a testing and validation phase, where manual supervision and control is desirable.

There are several necessary computational steps and algorithms involved in the workflow. The first one is the image processing for locating the workpiece on the table. Since the table will not always remain clean and shiny, the lighting changes in the course of the day and the system should be able to measure hot, cold and even cleaned workpieces, it can be challenging to reliably detect the workpiece boundaries. To simplify this task, the above-mentioned option to capture the empty table was included, in order to more easily separate workpiece from background. Figure 3 shows the network used for determining the position of the workpiece on the table, which was implemented using the Xeidana image processing library [22].

The key elements of this network are the following. The masking uses the reference background image and a black mask with a round transparent hole to remove all pixels outside the table. The actual workpiece detection is done via the threshold and blob analysis blocks, which identify large, connected sections of the table, which differ markedly from the background image. Finally, minimal rectangles are computed around this geometry to identify the workpiece center and orientation. The threshold can be supplied with different parameter sets to reliably identify, e.g., (dull grey or red hot) forged and (silvery shiny) cleaned workpieces.

The next interesting aspect is the generation of the motion path, which in this case, is a simple grid pattern. To generate a suitable path, the following variables are needed:

- The height of the table ztable,
- The width of the scanning line,
- The distance between scanning lines or the scan line overlap,
- The tilt angle of the scanner,
- The length, width and height of the workpiece (lwp, wwp, hwp),
- The location of the center of the workpiece,
- The orientation of the workpiece in the x-y-plane,

- The scan area enlargement,
- The speeds for positioning and scanning,
- Two suitable points near a flat empty surface for synchronization.

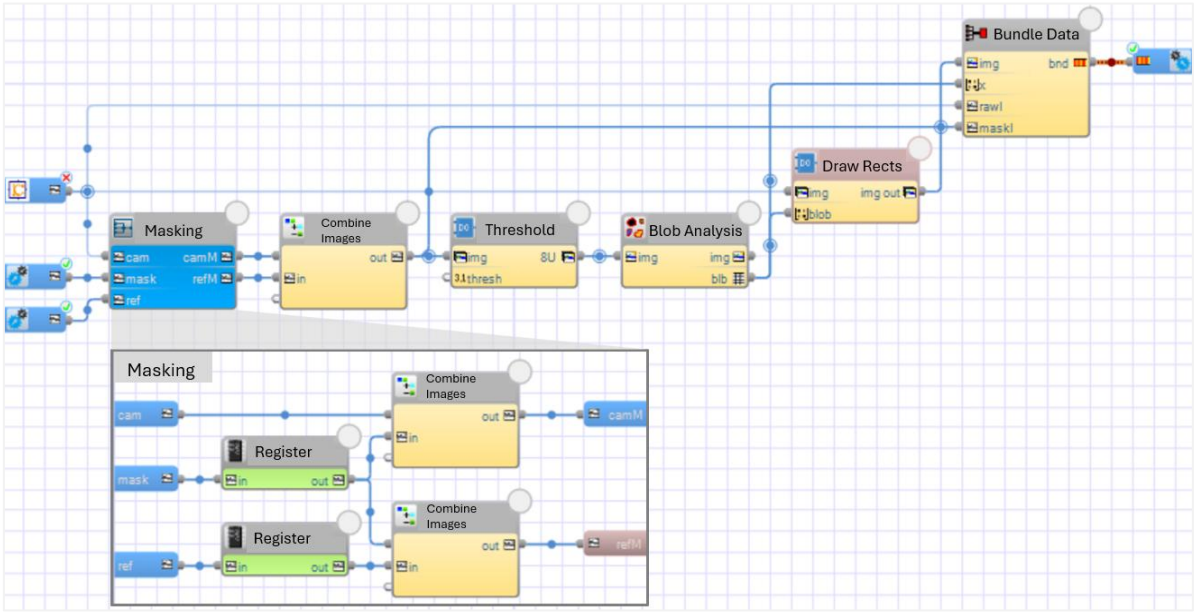


Fig. 3. Image processing network for object localization

The number of variables already shows that calculating a good path, even if only grid shaped, is not a simple matter. For a laser scanner, the scanning line is actually a cone, so its width depends on the distance between sensor and workpiece. For simplicity, we tried to work as much as possible with only a single constant z-position (height) for the scanning operation, so that all scanning movements are essentially in 2D:

$$z_{scan} = \max\left(z_{table} + 330 \cdot \cos(\beta)\,;\, z_{table} + h_{wp} + 150 \cdot \cos(\beta)\right), \tag{1}$$

For flat workpieces, we position the scanner as high as possible but low enough to just detect the top of the table surface. This way, we get a wide scanning line. For high workpieces, we take the height of the workpiece as a reference and make sure that the edge of the scanning range starts just above this height.

The angle β is the tilt angle of the scanner. Many workpieces have steep or even vertical flanks, which can only be reached with a tilted scanner. In our experiments, a 15° tilt worked well for most workpieces, but this is adjustable in the settings. Scans should overlap slightly to ensure a complete coverage of the workpiece, where overlaps between 5 and 20% are sensible. The tilt also necessitates longer scan paths to ensure complete coverage of the workpiece sides.

The position and orientation of the workpiece are determined from the image processing algorithm. They are, however, never exact, so that an area enlargement should be chosen to ensure that the complete workpiece is being scanned. 10 - 20% worked for us.

Speeds for scanning and positioning are important, because they determine the duration of the scanning process and its accuracy. A scan speed between 100 and 150 mm/s worked

well for us. The positioning speed should be high or even the maximum possible. The two different speeds also make it easier to distinguish between scanning and positioning in the robot position log files.

In theory, a separate synchronization of robot and scanner data should not be needed. In practice however, we have seen varying offsets of up to 80ms, which may be due to the communication via the Windows 11 operating system. To facilitate the synchronization before each scan, we let the robot move in a linear path towards the side wall of the room and then suddenly reverse direction. This reversal is easy to find in both the scanner data and the robot log data, which provides the time offset between both.

Using the workpiece orientation, a lengthwise and a perpendicular width wise scan direction are calculated as normalized 2D vectors. The scanning process starts with the synchronization move, then the TCP is moved to the lower left corner of the workpiece with position adjustments for the area enlargement, the scanning width and the scanner tilt. Then, a lengthwise linear scan followed by a perpendicular transition to the next path and another lengthwise scan in the opposite direction parallel to the first one. This is repeated until the right edge of the workpiece has been scanned. Afterwards, the scanner is rotated by 90° and the same procedure is repeated for the width wise scans.

An alternative, which has shown better accuracy at the cost of a slightly longer scan time is the unidirectional scanning, where after each scan, the scanner returns to the front edge for the next scan. This avoids some problems from small errors in the synchronization or the robot kinematics. Figure 4 shows both methods in the top two drawings.

The previously described option of using the part's orientation to define the two perpendicular scan directions offers very good scanning results with minimal scanning paths, at least in theory. However, as mentioned in Chapter 2, we have sometimes encountered the problem of collisions between robot and scanner, which are difficult to avoid in a fully automated workflow. They are also very dangerous, since they generally occur in the positioning movements, where the robot is particularly fast. Therefore, we have simplified the scanning path to make it more predictable and thus safer. This was done by defining fixed scan directions based only on the workpiece position rather than its orientation. We use the vector from the robot base to the workpiece center as the first 2D vector and the second vector is perpendicular to that, as seen in figure 4, lower left. In consequence, we now have predictable scanner orientations relative to the robot's configuration. The cost is that we need the operator to place the workpiece with its long axis in tangential orientation to the table, rather than simply randomly. This is necessary so that the length of the scanning paths can directly be calculated from the workpiece dimensions and the workpiece can be scanned completely in the shortest possible time.

Another option, which we have not yet tested, but which may offer better precision, is the use of circular scanning paths comparable to a windshield wiper on a car. Such a path, though less efficient, would require the movement of less robot axes for each path, see Fig. 4, lower right.

After the scanning, the data is exported and evaluated. The first step is to calculate the synchronization offset by searching the data for the reversal point. This point is easy to find, since it is also the position with the lowest y-coordinate in the recorded robot data, because the wall was used for the synchronization. With the offset, we can synchronize the entire robot

and scan data. Step two is identifying the parts of the robot data where a linear movement at scanning speed occurred for more than one second. These intervals represent the actual scanning, for which the corresponding scan data is retrieved. The robot positions are interpolated in time to match the exact moment each scan line was recorded. Then, the scan lines, which are arrays with z- and x-coordinates, are transformed into world coordinates using homogeneous transformation matrices calculated from the 6D cartesian robot coordinates. Typically, an additional transformation is required before this, to account for the constant offset between the robot's perceived tool center point (TCP) and the actual position and orientation of the scan line. This offset can be determined by scanning defined calibration targets or simply the smooth table surface with its holes and edges. The offset itself can then be calculated by formulating a least squares problem or more simply through trial and error. Once all scan points have been transformed into the world coordinate system (WCS), which is the robot coordinate system (RCS) in our case, then the next step depends on the quality of the calculated offsets.

If they are perfect, then all data points in overlapping scan regions should match and the evaluation can begin immediately. Otherwise, the individual scans can also be registered before the evaluation. This is what happened for us. We were able to combine all scans with the same orientation directly and had to register the resulting four point clouds in order to combine them correctly. The registration, depending on how closely the data is already aligned, is done first via the coarse RANSAC, followed by the finer ICP algorithms [23]. They choose smaller subsets of the typically very large point clouds to find optimal transformations for matching the datasets. The evaluation is finally just another registration, where the workpiece, exported as a triangular mesh is registered with the measured data. Using the position and orientation of the workpiece determined from the camera image, a good initial transformation can be applied before the registration, which speeds up the process.

Overall, a regular hp laptop from 2018 takes about 5 minutes to complete the entire data processing and evaluation for a workpiece of size 300mm by 500mm. One bottleneck is that we used python's open3d library for the registration, which takes quite long. A full integration of the registration in the software as precompiled code would speed up the calculation significantly.

One last important aspect of the solution is the implementation within the robot controller IRC5. We have a main module with a variable "programNumber" and a function "main()", which is repeatedly executed. This function checks the value of programNumber and calls subfunctions stored in separate modules depending on the desired action. The software can set the programNumber to, e.g., turn the rotary table, start the scanning process, move to the home position or even perform coordinate transformations on specified coordinates. The scanning process is stored in a module called "mainScanning", which is overwritten with the current path during the path planning step by the CAM software. This module, which is essentially the relevant NC code, is logged along with the robot and scan data for later analysis. This simple layout makes the system easy to both program and operate from within the CAM software. Additionally, the software RobotStudio can be used to simulate the motion path for the given robot configuration (see Fig. 5), which simplifies the commissioning phase.

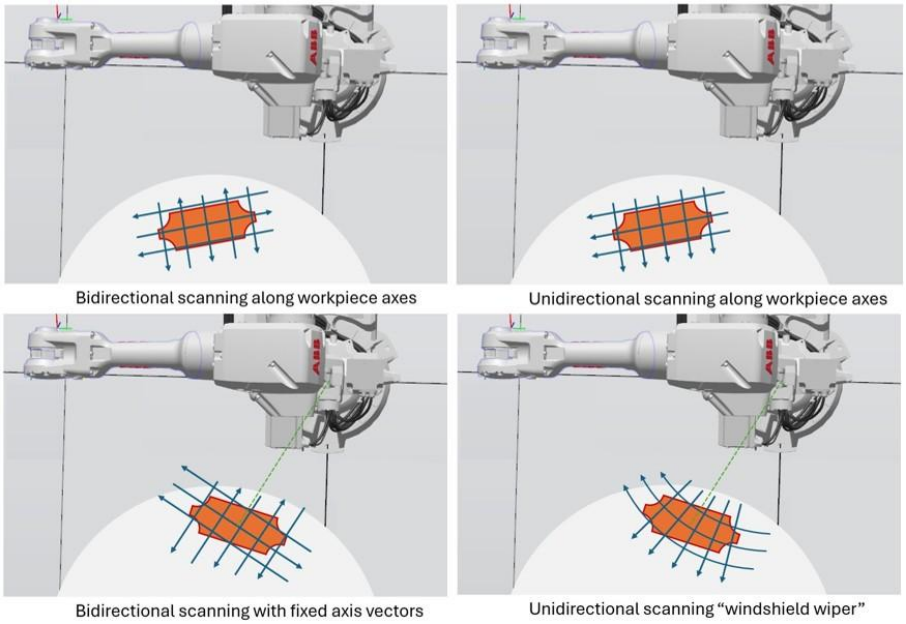


Fig. 4. Different path planning strategies

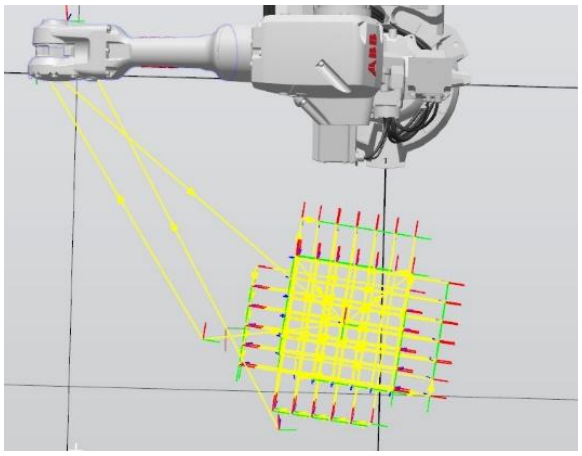


Fig. 5. Screenshot from RobotStudio for CAM path verification

4. MEASUREMENT PRECISION AND ERROR ANALYSIS

THE MEASUREMENT PRECISION depends on several factors, of which the precision of the robot plays a dominant role. We can assume that the scanner itself is precise enough, however the transformation and registration of the scanned data are two other factors with a large impact on the final result.

According to the product specifications and an ISO 9283 measurement, the ABB IRB 2600-20/1.65 has a positioning single-sided repeat precision of 0.04mm with an average single-sided absolute precision of 0.03mm. For linear paths, the single-sided repeat tolerance is 0.13mm with a single-sided absolute tolerance of 0.55mm. According to the ISO norm, these values were measured at a speed of 1.6m/s with the maximum tool load.

In order to gauge the actual accuracy of the robot beyond what the datasheet promises, a measurement with a FARO ION laser tracker was performed. The laser tracker was placed on the table at a distance of about 2.5m to the robot. To track the robot's movement, a magnetic optical reflector was placed on the side of the scanner housing. This does not allow for precise measurements of the tool center point (TCP) precision, but it gives a good sense of the precision during linear scanning movements with a constant tool orientation. Ideally, the scanner should be removed and replaced with a specialized mounting, which provides a defined 1D z-offset to the actual robot TCP. However, removing and reattaching the scanner might change the calibration offset and the tool weight would be different, which would reduce the usefulness of the measurement. The largest drawback of the measurement is the inability to distinguish between translational and rotational errors by measuring only 3D rather than 6D. Here, a GOM Aramis or similar system with markers placed on the scanner would be a better option.

Since we were mostly interested in the path accuracy for the linear scanning paths in the reachable area above the rotary table, we created realistic scanning paths for two different locations on the table and tracked the scanner movement along these paths at different speeds and for both the bidirectional and unidirectional scan routines. More specifically, we wanted to see how well the laser tracker data matched the robot log data in motion, how the precision changed for increased scanning speeds, if there is a difference between unidirectional and bidirectional scanning and if the precision changes with the workpiece location on the table.

Figure 7 shows the difference between laser tracker and robot data for a scan with 100mm/s, whose position data is shown in Fig. 6. We can clearly see a static stiffness error in all three coordinates but most dominantly in the z- and x-coordinates. For example, in the first 10s, the scanner moves in the x-direction and we see a nearly linear dip in the z-coordinate by as much as 1.5mm as measured by the laser tracker. Similarly, there is a wide z-dip of ca. 1mm in the entire second half of the measurement. This was expected since we do not know the exact weight of the scanner plus cooling mantle, mounting, coolant and cables. This makes ABB's internal stiffness compensation ineffective.

Based on these curves, the linear compensation in equation 2 was applied, which yielded the compensated curves shown in Fig. 8. The m, n and f are constants, where m is a slope and n is the intercept of the linear equation. f is simply a factor to correlate the strong vertical to the weak horizontal stiffness error. L_{xy} is the distance from the robot base to the projection of the center of robot axis 5 onto the x-y-plane, essentially how far the robot stretches horizontally. dL_{xy} is the difference between the robots actual (x,y)-TCP and L_{xy}, which accounts for different tilts of the relatively heavy scanner. Finally, the angular terms in the x and y equations account for the position of robot axis 1, which determines how much of the horizontal stiffness error affects the x and how much the y-coordinate.

$$dx_{stiff} = (L_{xy} - n_1) \cdot (m_1 \cdot f + (n_2 - dL_{xy}) \cdot m_2) \cdot \cos\left(\tan^{-1}(y/x)\right) \tag{2a}$$

$$dy_{stiff} = (L_{xy} - n_1) \cdot (m_1 \cdot f + (n_2 - dL_{xy}) \cdot m_2) \cdot \sin\left(\tan^{-1}(y/x)\right) \tag{2b}$$

$$dz_{stiff} = (L_{xy} - n_1) \cdot -(m_1 + (n_3 - dL_{xy}) \cdot m_3) \tag{2c}$$

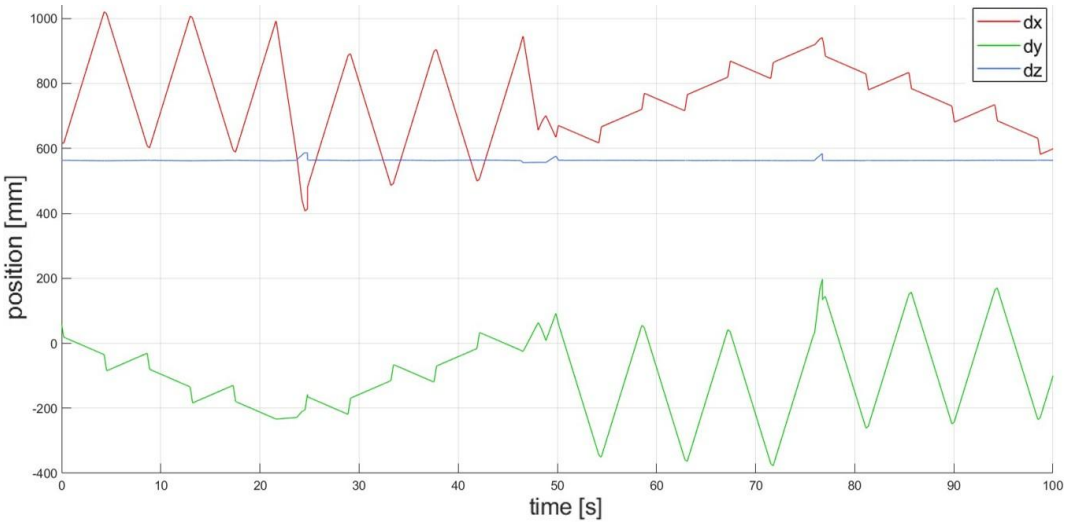


Fig. 6. Position data from robot log for bidirectional scanning

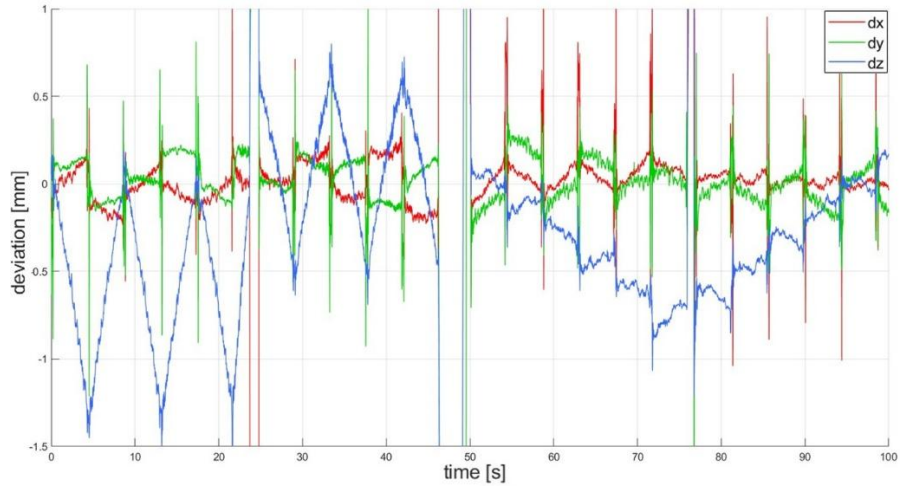


Fig. 7. Position deviation between laser tracker and robot for bidirectional scanning

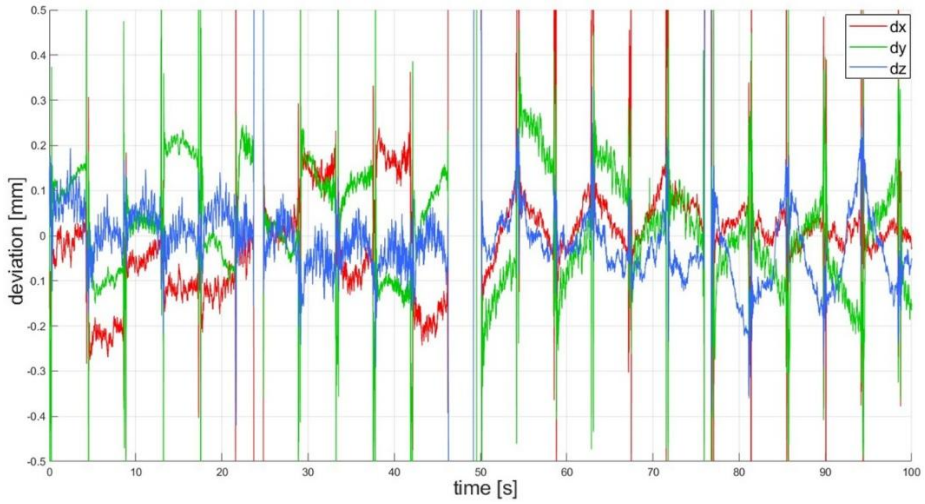


Fig. 8. Deviation between laser tracker and compensated robot position

The constants were determined via regression analysis and showed a similar effectiveness across all scanning speeds and all investigated workpiece positions. The compensated data still shows notable systematic errors, but these are close to the position uncertainty of the robot and no better compensation algorithm was likely to be found with the measurement setup used here. Better results may be possible with a sensor capable of measuring the scanner position in 6D, such as the GOM Aramis, or by switching to the simpler windshield wiper CAM strategy.

The corresponding curves for scanning speeds of 50mm/s and 170mm/s show both qualitatively and quantitatively the same deviations. Thus, the scanning speed does not influence the accuracy of the robot within the investigated range, though more speed means less density of the scan lines. Still, since the scanning frequency of the scanner is high enough and in order to minimize the scanning duration and the workpiece cooling during the scanning process, fast scanning is recommended.

With the precision of the robot determined and within an acceptable range, the next step is to verify the scan data of an actual part by comparing it to a precise commercial scanning system. In this test, a cold part was used in order to ensure that the geometry of both scans is identical. The test was performed with the Steinbichler T-Scan, which is a hand-held laser triangulation-based sensor, whose position in space is constantly tracked via a stationary stereoscopic tracking bar. The datasheet of the T-Scan mentions an average point distance of 0.075mm but gives no clear values on its measurement uncertainty. Assuming an uncertainty comparable to other industrial systems, such as GOM ATOS or Nikon D800, the value will be in the range of 0.1 - 0.2mm, depending on the distance between tracker and scanner, the object shape, the measurement procedure and the precision of the registration process [24].

For the test, a cleaned part with a rectangular shape of around 200x300mm in size with cylindrical peg and a wide furrow in the top middle section was used. The part was first scanned using the T-Scan in the lab. The scan data was merged, triangulated, cleaned and exported as an STL model. Afterward, the part was placed on the rotary table in the measurement room and scanned again by the robot-held laser scanner. After importing the STL file as the target model, the inspection software can directly compute the deviation between both models. Figure 9 shows the measurement of the part in the lab using the T-Scan on the left and the part on the rotary table both top and bottom on the right.

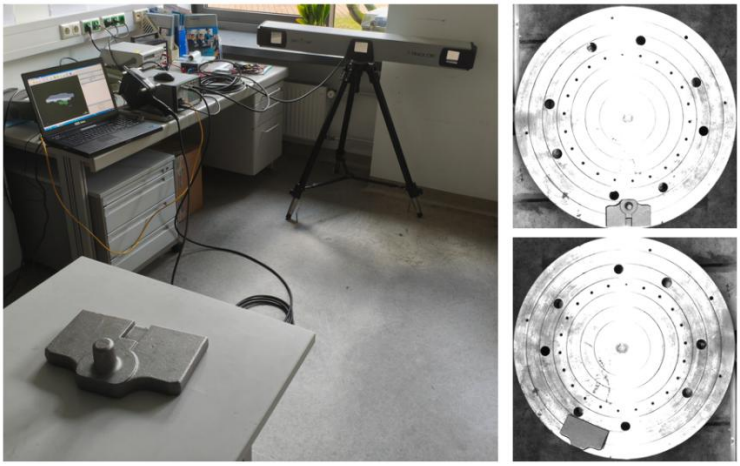


Fig. 9. Scan data deviation between robot-held scanner and Steinbichler T-Scan

Figure 10 displays the differences between both scans in a screenshot from the software. The right part shows the position of the 1000 randomly chosen colored evaluation points amidst the grey reference model points.

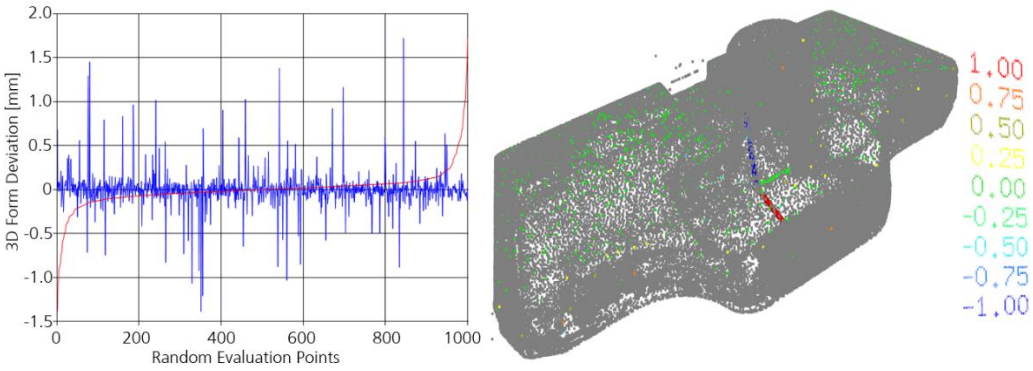


Fig. 10. Scan data deviation between robot-held scanner and Steinbichler T-Scan

The left chart shows the geometric deviation between both scanners, which ranges from -1.4mm to 1.7mm with an average of 0.0mm and a standard deviation of 0.2mm. The red line is the same data as the blue line but sorted from lowest to highest. Overall, 72% of the data is withing +/- 0.1mm, 96% within +/- 0.5mm and 99% within +/- 1.0mm. Most of the larger deviations are clearly identifiable as outliers.

Using a different part (see Fig. 1, right), which was fully cooled but not cleaned, the influence of the results with different CAM parameters was tested. The measured part was a failed part with large deviations. This allowed us to assess, if different scans showed the same deviations in the same regions. We compared scanning at 100mm/s and 140 mm/s for both unidirectional and bidirectional scans and at three different locations on the table. The reference was the CAD model of the cold part. The scan results for bidirectional paths and 100mm/s scanning speed are shown in Fig. 11.

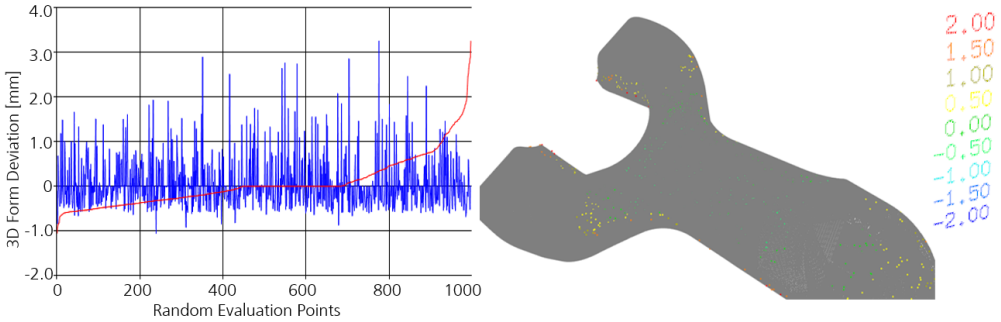


Fig. 11. Scan data deviation between robot-held scanner and CAD model

The deviation ranges from -1.1mm to +3.3mm, though these figures are strongly inflated by individual outliers. We see some larger deviations both near the two prongs on the left as well as near the tip on the right (compare fig. 11 right). Here, only 75% of the data is within +/- 0.5mm with 93% within +/- 1.0. The data also shows an asymmetry, so that 93% of the

evaluated points are also within (-0.6, 1.2). In practice, this means that the part is actually slightly larger than it should be. Comparing figures 10 and 11, the 2D chart shows the user at a single glance if there is a chance of the part being out of tolerance and the 3D error map allows the user to pinpoint the deviation on the part. Isolated outliers can be ignored.

When comparing different scan parameters and locations of the same part, we see nearly identical results. While a direct comparison of different scans is not possible due to registration and randomized evaluation, the results show no indication of a dependence on any of the investigated factors mentioned above.

Another aspect revealed by our initial tests, is that the automated registration often fails, if the target point cloud is directly created from the vertices of the STL model of the workpiece. The STL model is the triangulation of the CAD geometry, which is typically created from a STEP model. Particularly with large, flat workpieces, there will be large sections of the surface represented by very few large triangles. The resulting sparse point clouds make registration difficult or even impossible. To resolve this, an iterative refinement algorithm was included in the software, which reduces the sizes of all triangles larger than a specified threshold (e.g. 5mm) evenly by roughly a factor of 2-3 in each step. Figure 12 shows the mesh for the inner center portion of a bowl-shaped part before and after one mesh refinement step. This first step increased the mesh from 53,292 faces and 26,648 nodes to 128,786 faces and 102,142 nodes.

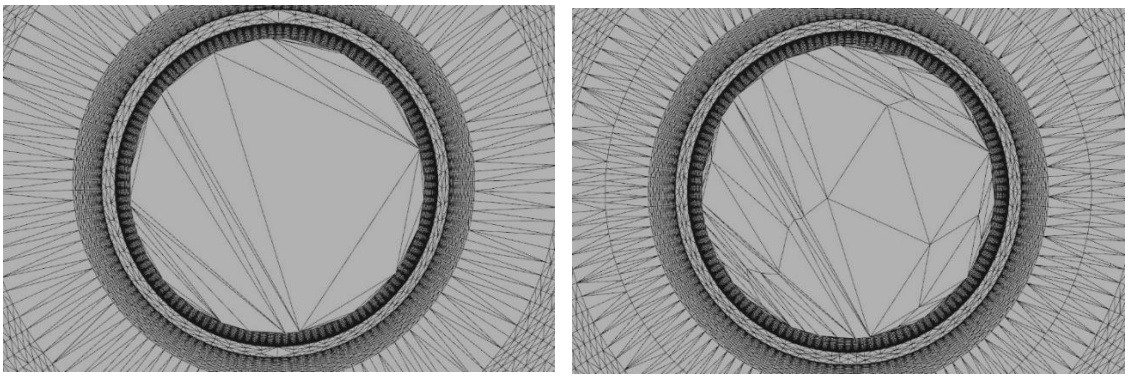


Fig. 12. Original triangle mesh (left) and mesh after one refinement step (right)

As previously stated, the forging environment may always experience some vibrations from nearby forges. These hammer strikes lead to loud noise and noticeable shaking in the adjacent measurement room, even when the room is closed off. Truly relevant is, however, only how much this influences both the workpiece on the rotary table and the robot on the concrete foundation.

Figure 13 shows the measured movement of the target on the robot as viewed from the laser tracker during particularly strong strikes. The robot was in home position, see Fig. 1. The graphs show oscillations with an amplitude of about +/-0.025mm in x and y direction and about +/-0.05mm in z direction. In the overall precision range of the system, these oscillations are acceptable but should still be avoided whenever possible and otherwise considered during the data interpretation. It should also be noted that these values apply to the home position and may be larger in fully extended robot poses.

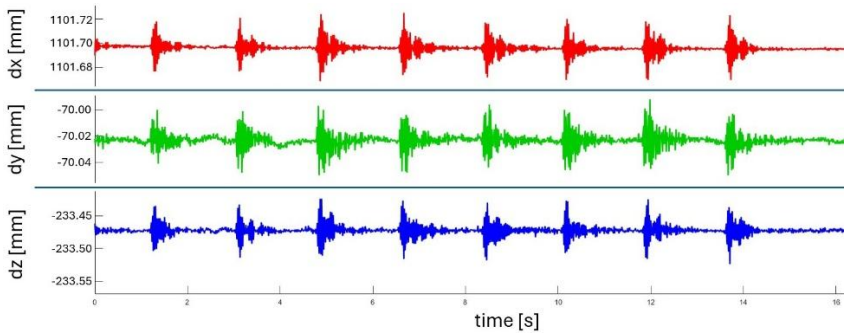


Fig. 13. Hammer strikes within laser tracker position data

Filtering is possible but may also just replace one error with another, since we cannot assume that the surface scanned during the impacts is smooth or flat. The best option seems to make note of forging strikes occurring during the scanning process. If large deviations are subsequently detected in the data, then the measurement should be repeated. If the forging strikes are continuous, then the results of the repeat measurement should be compared to the first results to check if the deviations are seen in the same location or perhaps instead are wandering.

Table 2 summarises the errors from the different sources but cannot yet ultimately present a clear measurement uncertainty. Further research and a statistically significant number of measurements confirmed by a more precise external system are required.

Table 2. Error estimates for the inspection system

Error Source	Estimated Error	Remarks
Robot positioning uncertainty	+/- 0.25 mm in x/y/z	After stiffness compensation
Synchronization error robot - scanner	negligible	Synchronization routine removes error almost completely; registration removes remaining offsets
Offset from robot TCP to scanner origin	negligible	Calibration reduces offset to less than 1mm; registration removes remaining offsets
Precision of laser line scanner	0.01 mm in z x unknown	According to datasheet, not verified
Ambient vibrations	+/- 0.025 in x/y +/- 0.05 in z	May be higher for highly extended robot poses; typically avoidable
Model registration	Unknown	Depends on part shape, STL model fineness, error thresholds, scan data, etc.
Thermal error from part shrinkage	Unknown	Depends on part shape, temperature, measurement duration, precision of thermal sensor, simulation error, etc.
Total Uncertainty	Unknown, but observed to be around +/-1mm for cold workpieces	Mainly registration and thermal errors are unknown and make estimations difficult

5. SUMMARY AND CONCLUSION

FORGING is an important process for the manufacture of many industrially relevant products from automotive, railway and aerospace to defence sectors. Particularly in safety-relevant applications, the quality tolerance can be quite narrow. Meeting these tolerances requires not only good planning and control of the entire forging process but also the subsequent quality inspection of the produced parts.

The paper starts by exploring different solutions available in the state of the art, which range from simple mechanical gauges to various 3D scanners. Next, the challenges for a cost-effective industrial application are listed. Of these, the most problematic are the high temperatures of up to 1000°C, the high degree of automation and the large geometric variability of the parts. A hardware concept comprised of a robot holding a laser line scanner and a rotary table is proposed, which is subsequently integrated into a measurement room adjacent to the production hall close to the forge.

The main steps of the quality inspection process include the rotation of the workpiece to directly in front of the robot, detecting the object location via a 2D camera, planning a grid-shaped scanning path across the part's dimensions, exporting, synchronizing and transforming the scan data and registering the data against a target CAD model. These steps along with the required support and communication structure have been implemented in a custom CAM software, which is briefly described. The key challenges include the automated object localization, the motion path planning and the data evaluation.

The final chapter investigates the measurement precision of the system and thereby evaluates the feasibility of the approach. In a first step, the precision of the robot was verified using a laser tracker. The measurement initially revealed a large static error, which likely resulted from the tool weight. Using a linear compensation, the measured precision of the robot in motion for simulated scan paths was improved to +/-0.25mm in all three dimensions.

Next, the scanned geometry for a part was compared to the more accurate commercial system Steinbichler T-Scan. The test showed a good agreement between both systems with 96% of the data lying within +/- 0.5mm.

Using another forged part, the impact of different CAM strategies and scanning speeds were tested, which showed no noticeable effect within the investigated parameters. Both unidirectional as well as bidirectional scanning created nearly identical scans, when the proper data synchronization routine was used to account for time lag between scanner and robot. Likewise, the robot speed, tested for 100mm/s and 140mm/s, produced the same results.

A final investigation measured the impact of nearby hammer strikes from forges on the measurement system. These showed an amplitude of up to +/-0.05mm but may also be higher for fully extended robot poses.

In the conclusion, we should ask whether the developed inspection system satisfies the requirements formulated in chapter 2. The automated scanning of relatively large, hot forgings is generally possible with the proposed system. It is not currently fully automated, especially since the part handling remains a manual task requiring a forklift and manual control. Further automation is possible but would be neither simple nor cost effective for this production environment. All other steps from inspection planning to data evaluation are fully automated and only require CAD models for referencing.

The cycle time depends on the part and the PC used for data processing. With the current setup, two-sided scans including logistics and evaluation take around 10 minutes for medium sized parts. A faster PC, well-rehearsed staff and some optimization in the path planning and evaluation could potentially lower this to 6-8 minutes but the envisioned 3-5 minutes are not feasible. This is still acceptable, especially if only every second or third part needs to be measured.

The high temperatures can be problematic, particularly due to the short measuring distance of the laser scanner. IR filters will, however, likely solve this problem. The system is also affordable, if the relatively high development effort is neglected. Building a second system, even with different hardware and setup will only require minor changes to the CAM software.

The measurement uncertainty will not reliably be under 0.5mm, but 1.0mm is very realistic and the average deviations have been well below 0.5mm. For forgings, this is generally adequate. Table 3 compares the current performance of the inspection system to the initial expectations and goals set in chapter 2. Overall, the great flexibility and high degree of automation of the system along with its good accuracy make it a valuable tool for checking the workpiece geometry of hot forgings and thereby avoiding unnecessary scrap and emissions in the case of failed parts.

Table 3. Performance Check

☑ / ☒	Criterion	Remarks
☑	Parts of varying shapes up to a size of 0.8m x 0.8m x 0.3m	Demonstrated for this size; scalable via larger table and robot
☑	Suitable for small to medium batch sizes	Very low setup effort for new parts
☒	Cycle time including logistics < 5min, ideally <3min	Scanning and data evaluation depend on the size of the part; currently up to 10 minutes, but can be optimized/reduced
☑	Initial part temperature variable, up to 1000°C	System designed for high temperatures; IR-filters will be retrofitted for robustness
☑	Vibration-resistant measurements	Vibrations do have an effect, but are typically low enough to ignore
☑	Hardware cost < €100,000	Neglecting personnel cost for R&D and commissioning
☑	Automated procedure	Mostly automated: Manual loading / unloading and turning of parts; manual triggering and supervision for safety
☒	Measurement uncertainty < 1mm, ideally < 0.5mm	Tests on cold parts indicate this level of precision but cannot be guaranteed for hot parts

Future research will focus primarily on two aspects. The first is the further testing and optimization of the system with the aim of making the scanning process faster, more robust

and more accurate. This includes the installation of IR filters and the porting of the registration to C++ or similar compiled code.

The second aspect is the investigation and handling of the thermal shrinkage. Steel expands with ca. 12 µm/mK, so that parts of 0.5m diameter will shrink by as much as 6mm during their cool-down. Currently, we simulate the thermal expansion and use the expanded geometry of the part as refence, rather than its cold CAD geometry. This is, however, not very exact, since the temperature of the part during scanning can vary, e.g. due to delays in the logistics. We measure the temperature using pyrometers, but the temperature is not homogeneous and changes by as much as 50K even during the scanning process. This requires a better, more accurate approach, which ideally requires no separate thermal simulations.

REFERENCES

[1] RATHI M.G., JAKHADE N.A., 2014, *An Overview of Forging Processes with Their Defects*, Int. J. of Scientific and Research Publications, 4/6, 2250-3153.

[2] HAWRYLUK M., JAKUBIK J., 2016, *Analysis of Forging Defects for Selected Industrial Die Forging Processes*, Engineering Failure Analysis, Elsevier, 59, 396–409, https://doi.org/10.1016/j.engfailanal.2015.11.008.

[3] EMAMVERDIAN A.A., SUN Y., CAO C., PRUNCU C., WANY Y., 2021, *Current Failure Mechanisms and Treatment Methods of Hot Forging Tools (Dies) - a Review*, Engineering Failure Analysis, Elsevier, 129, 105678, https://doi.org/10.1016/j.engfailanal.2021.105678.

[4] REICHER R., 2011, *Robot Based 3D Scanning and Recognition of Workpieces*, Master Thesis, Örebro University.

[5] BROSED F.J., AGUILAR J.J., GUILLOMIA D., SANTOLARIA J., 2011, *3D Geometrical Inspection of Complex Geometry Parts Using a Novel Laser Triangulation Sensor and a Robot*, MDPI Sensors, 11/1), 90–110, https://doi.org/10.3390/s110100090.

[6] MEJIA-PARRA D., SANCHEZ J.R., RUIZ-SALGUERO O., ALONSO M., IZAGUIRRE A., GIL E., PALOMAR J., POSADA J., 2019, *In-Line Dimensional Inspection of Warm-Die Forged Revolution Workpieces Using 3D Mesh Reconstruction*, MDPI Applied Sciences, 9/6, 1069, https://doi.org/10.3390/app9061069.

[7] LAZAREVIC D., NEDIC B., JOVIC S., SARKOCEVIC Z., BLAGOJEVIC M., 2019, *Optical Inspection of Cutting Parts by 3D Scanning*, Physica A, 531, 121583, https://doi.org/10.1016/j.physa.2019.121583.

[8] HAWRYLUK M., ZIEMBA J., 2016, *Possibilities of Application Measurement Techniques in Hot Die Forging Processes*, *Measurement*, Elsevier, 110, 284–295, https://doi.org/10.1016/j.measurement.2017.07.003.

[9] DA SILVA SANTOS K.R., DE OLIVEIRA W.R., VILLANI E., DTTMANN A., 2023, *3D Scanning Method for Robotized Inspection of Industrial Sealed Parts*, Computers in Industry, 147, 103850, https://doi.org/10.1016/j.compind.2022.103850.

[10] HAN S., DO M.D., KIM M., CHO S., CHOI S.-K., CHOI H.-J., 2022, *A Precise 3D Scanning Method Using Stereo Vision with Multipoint Markers for Rapid Workpiece Localization*, Journal of Mech. Science and Technology, 36/12, Springer, 6307–6318, http://doi.org/10.1007/s12206-022-1142-2.

[11] LI Z., LIU X., WEN S., HE P., ZHONG K., WEI Q., SHI Y., LIU S., 2018, *In Situ 3D Monitoring of Geometric Signatures in the Powder-Bed-Fusion Additive Manufacturing Process Via Vision Sensing Methods*, MDPI Sensors, 18/4, 1180, https://doi.org/10.3390/s18041180.

[12] TIAN Z., GAO F., JIN Z., ZHAO X., 2009, *Dimension Measurement of Hot Large Forgings with a Novel Time-of-Flight System*, Int. J. of Adv. Manuf. Techn., 44, 125–132, https://doi.org/10.1007/s00170-008-1807-8.

[13] BOKHABRINE Y., SEULIN R., VOON L.F.C.L.Y., GORRIA P., GIRARDIN G., GOMEZ M., JOBARD D., 2012, *3D Characterization of Hot Metallic Shells During Industrial Forging*, Machine Vision and Applications, 23, 417–425, https://doi.org/ 10.1007/s00138-010-0297-5.

[14] DU Z., DU Y., 2012, *Simple Three-Dimensional Laser Radar Measuring Method and Model Reconstruction for Hot Heavy Forgings*, Optical Engineering, 51/2, https://doi.org/10.1117/1.OE.51.2.021118.

[15] LIU W., JIA X., JIA Z., LIU S., WANG B., DU J., 2011, *Fast Dimensional Measurement Method and Experiment of the Forgings Under High Temperature*, Journal of Material Processing Technology, 211, 237–244, https://doi.org/10.1016/j.jmatprotec.2010.09.015.

[16] LIU W., JIA Z., WANG F., MA X., WANG W., JIA X., SONG D., 2012, *An Improved Online Dimensional Measurement Method of Large Hot Cylindrical Forging*, Measurement, 45, 2041–2051, https://doi.org/10.1016/j.measurement.2012.05.004.
[17] LIU Y., JIA Z., LIU W., WANG L., FAN C., XU P., YANG J., ZHAO K., 2016, *An Improved Image Acquisition Method for Measuring Hot Forgings Using Machine Vision*, Sensors and Actuators A: Physical, 238, 369–378, https://doi.org/10.1016/j.sna.2015.11.035.
[18] ZHANG Y.-C., HAN J.-X., FU X.-B., LIN H.-B., 2014, *An Online Measurement Method Based on Line Laser Scanning for Large Forgings*, Int. J. of Adv. Manuf. Techn., 70, 439–448, https://doi.org/10.1007/s00170-013-5240-2.
[19] ZHANG Y.-C., HAN J.-X., FU X.-B., ZHANG F.-L., 2014, *Measurement and Control Technology of the Size for Large Forgings*, Measurement, 49, 52–59, https://doi.org/10.1016/j.measurement.2013.11.028.
[20] ZHAO X., LIU J., ZHANG H., WU Y., 2015, *Measuring the 3D Shape of High Temperature Objects Using Blue Sinusoidal Structured Light*, Meas. Sci. Techn., 26, 125205, https://doi.org/10.1088/0957-0233/26/12/125205.
[21] HAN L., CHENG X., LI Z., ZHONG K., SHI Y., JIANG H., 2018, *A Robot-Driven 3D Shape Measurement System for Automatic Quality Inspection of Thermal Objects on a Forging Production Line*, MDPI Sensors, 18/12, 4368, https://doi.org/10.3390/s18124368.
[22] Xeidana, https://www.xeidana.de/de/xeidana.html
[23] Open3D Documentation, https://www.open3d.org/docs/0.19.0/tutorial/pipelines/global_registration.html
[24] KERSTEN T.P., PRZYBILLA H.-J., LINDSTAEDT M., TSCHIRSCHWITZ F., MISGAISKI-HASS M., 2016, *Genauigkeitsuntersuchungen Handgeführter Scanner*, Dreiländertagung der DGPF, OVG und SGPF, 25, 271–287.